Gradient-Based Predictive Pulse Pattern Control with Improved Steady-State and Dynamic Behavior

Ilari Hilden
Faculty of Inf. Technol. and Commun. Sciences
Tampere University
Tampere, Finland
ilari.hilden@tuni.fi

Petros Karamanakos
Faculty of Inf. Technol. and Commun. Sciences
Tampere University
Tampere, Finland
p.karamanakos@ieee.org

Tobias Geyer
Motion System Drives
ABB Switzerland Ltd
Turgi, Switzerland
t.geyer@ieee.org

Shirin Rahmanpour
Faculty of Inf. Technol. and Commun. Sciences
Tampere University
Tampere, Finland
shirin.rahmanpour@tuni.fi

***Abstract*—This paper presents an optimal control strategy for grid-connected converters with LCL filters. Specifically, a gradient-based model predictive control (MPC) scheme is developed to manipulate optimized pulse patterns (OPPs) in real time such that very low grid current harmonic distortions are achieved even at switching frequencies close to the filter resonance frequency. To fully exploit the potential of OPPs—in terms of their ability to produce very low harmonic distortions—optimal steady-state reference trajectories are derived based on the OPP in use. Thanks to this, the proposed MPC scheme achieves excellent steady-state performance by producing the optimal output ripple. However, the rigid nature of OPPs may lead to the underutilization of the converter voltage margin during transients. To avoid this, a three-phase pulse insertion strategy is proposed wherein the OPP is locally overwritten such that the switch positions that can result in a very fast dynamic performance become available to the controller. The effectiveness of the proposed control strategy is verified with a system consisting of a two-level converter connected to the grid via an LCL filter.**

***Index Terms*—Grid-tied converters, model predictive control (MPC), optimized pulse patterns (OPPs)**

I. Introduction

Converters connected to the grid have to meet specific harmonic grid standards and produce (very) low grid current total demand distortion (TDD). For this reason, they are typically connected to the grid via LCL filters that can effectively attenuate harmonics above the filter resonance frequency. The control problem of the resulting multiple-input multiple-output (MIMO) system is commonly addressed by multiple single-input single-output (SISO) control loops designed in cascade [1]. These different loops, however, tend to interact with each other in an adverse manner during transients, thus limiting the controller bandwidth [2]. Moreover, the use of conventional modulation techniques, such as carrier-based pulse width modulation (CB-PWM) and space vector modulation (SVM), can pose further challenges [3]. Specifically, the switching-to-filter resonance frequency ratio should be relatively high, e.g., at least three, to ensure sufficient bandwidth of the closed-loop system [4], [5]. This limitation can result in either an oversized filter, or an increased switching frequency, and, consequently, power losses.

Therefore, to achieve favorable steady-state and dynamic performance by means of control and modulation all the aforementioned challenges have to be considered. A promising solution is MPC with OPPs, as also shown in [6]. Such a combination enables the exploitation of the MIMO nature of MPC that allows for high bandwidth [7], and of the excellent steady-state performance of OPPs, with which the theoretical minimum current distortions can be achieved [8], [9]. In this direction, a method that combines MPC with OPPs—referred to as gradient-based predictive pulse pattern control (GP^{3}C)—was proposed for grid-tied converters with LCL filters in [10] and produced steady-state grid currents with low distortions. However, [10] assumes sinusoidal references for the controlled variables, meaning that the *optimal* ripple introduced by the OPPs is not considered. This forces the controller to take unnecessary actions to compensate for the instantaneous control error. As a result, the system output trajectories deviate from the optimal ones, thus increasing the harmonic distortions. Moreover, the use of sinusoidal references in [10] results in a cumbersome controller tuning process to account for the relative error among the output variables.

Additionally, the dynamic performance of the system is altogether neglected in [10]. The inflexible nature of OPPs, combined with the controller formulation, intrinsically does not allow for fast dynamic responses [11]. This is because GP^{3}C is limited to manipulating only the three-phase switch positions that are locally present in the OPP in a specific chronological order. Hence, the switch positions that can speed up the transient response are not always available, which compromises the dynamic performance of the system. This problem is especially aggravated when convoluted dynamics are involved, as is the case with the system in question [12].

Motivated by the above, this work revises the control method presented in [10] to improve the steady-state performance and achieve very fast transient responses. To this aim, optimal output reference trajectories are designed based on the OPP in use to ensure very low harmonic distortions in the grid current, while rendering the controller tuning redundant. Moreover, to achieve superior dynamic performance, the OPP is locally overwritten during transients by strategically inserting three-phase pulses that can fully utilize the available voltage margin. The presented comparisons with linear control

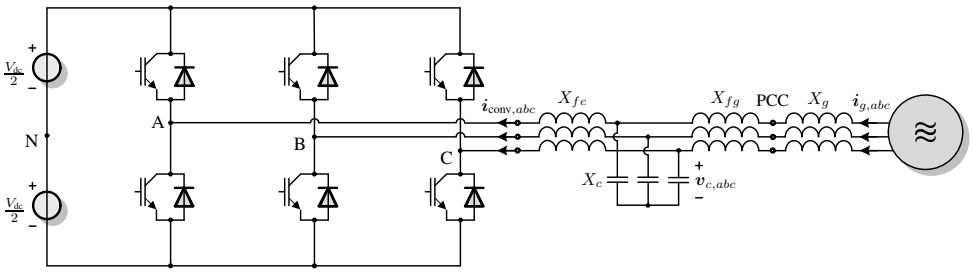

Fig. 1. Two-level grid-tied converter with an LCL filter.

with SVM demonstrate the benefits of the proposed control algorithm in steady state, while comparisons with finite control set MPC (FCS-MPC) [13], [14] show the effectiveness of the devised three-phase pulse insertion strategy during transients.

II. Model of the Grid-Tied Converter with an LCL Filter

The chosen case study relates to a two-level grid-tied converter with an LCL filter, as shown in Fig. 1. Assuming that the dc-link voltage V_{dc} is fixed, the output converter voltage in phase x, $x \in \{a, b, c\}$, can assume the values $-V_{\text{dc}}/2$, or $V_{\text{dc}}/2$, which correspond to the *single-phase* switch position $u_x = -1$, or $u_x = 1$, respectively.

As the controller is designed in the stationary orthogonal ($\alpha\beta$) reference frame, any three-phase variable $\boldsymbol{\xi}_{abc} \in \mathbb{R}^3$ is mapped into the $\alpha\beta$-plane through the linear transformation $\boldsymbol{\xi}_{\alpha\beta} = \boldsymbol{K}\boldsymbol{\xi}_{abc}$, where $\boldsymbol{\xi}_{\alpha\beta} \in \mathbb{R}^2$ is the variable in the $\alpha\beta$-plane, and $\boldsymbol{K}$ is the reduced Clarke-transformation matrix. Therefore, the converter output voltage $\boldsymbol{v}_{\text{conv}}$ can be derived from the *three-phase* switch position $\boldsymbol{u}_{abc} = [u_a \ u_b \ u_c]^T \in \{-1, 1\}^3$ as[1]

$$\boldsymbol{v}_{\text{conv}} = \frac{V_{\text{dc}}}{2}\boldsymbol{K}\boldsymbol{u}_{abc}\,. \tag{1}$$

Considering the equivalent circuit representation of the system in question (see Fig. 2), the following differential equations describe its dynamics

$$\frac{\mathrm{d}\boldsymbol{i}_{\text{conv}}}{\mathrm{d}t} = \frac{1}{X_{fc}}\left(\boldsymbol{v}_c - (R_{fc} + R_c)\boldsymbol{i}_{\text{conv}} + R_c\boldsymbol{i}_g - \boldsymbol{v}_{\text{conv}}\right) \tag{2a}$$

$$\frac{\mathrm{d}\boldsymbol{i}_g}{\mathrm{d}t} = \frac{1}{X_{gr}}\left(\boldsymbol{v}_g - (R_{gr} + R_c)\boldsymbol{i}_g + R_c\boldsymbol{i}_{\text{conv}} - \boldsymbol{v}_c\right) \tag{2b}$$

$$\frac{\mathrm{d}\boldsymbol{v}_c}{\mathrm{d}t} = \frac{1}{X_c}\left(\boldsymbol{i}_g - \boldsymbol{i}_{\text{conv}}\right) \tag{2c}$$

$$\frac{\mathrm{d}\boldsymbol{v}_g}{\mathrm{d}t} = \omega_g \begin{bmatrix} 0 & -1 \\ 1 & 0 \end{bmatrix} \boldsymbol{v}_g\,, \tag{2d}$$

where the parameters are the converter-side filter reactance (resistance) X_{fc} (R_{fc}), the filter capacitor reactance (resistance) X_c (R_c), and the equivalent reactance and resistance, $X_{gr} = X_{fg} + X_g$ and $R_{gr} = R_{fg} + R_g$, respectively, where X_{fg} (R_{fg}) and X_g (R_g) are the grid-side filter and grid reactances (resistances), respectively. Finally, ω_g is the angular grid frequency.

[1]Throughout this paper the subscript $\alpha\beta$ is omitted from the variables in the $\alpha\beta$-plane to simplify the notation. On the other hand, subscript abc is used to indicate the three-phase quantities.

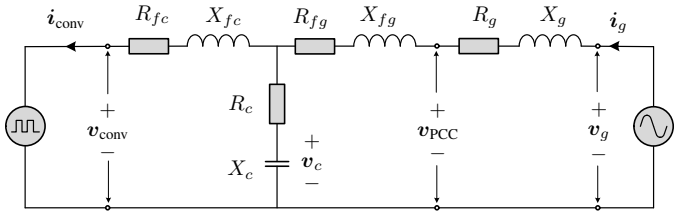

Fig. 2. Equivalent circuit of a two-level converter connected to the grid via an LCL filter in the stationary orthogonal ($\alpha\beta$) reference frame.

Let the three-phase switch position be the system input, the converter current, filter capacitor voltage, grid current, and grid voltage the system state, i.e., $\boldsymbol{x} = [\boldsymbol{i}_{\text{conv}}^T \ \boldsymbol{i}_g^T \ \boldsymbol{v}_c^T \ \boldsymbol{v}_g^T]^T \in \mathbb{R}^8$, and $\boldsymbol{y} = [\boldsymbol{i}_{\text{conv}}^T \ \boldsymbol{i}_g^T \ \boldsymbol{v}_c^T]^T \in \mathbb{R}^6$ the system output. With the help of (1) and (2), the continuous-time state-space model of the system is

$$\frac{\mathrm{d}\boldsymbol{x}(t)}{\mathrm{d}t} = \boldsymbol{F}\boldsymbol{x}(t) + \boldsymbol{G}\boldsymbol{u}_{abc}(t) \tag{3a}$$

$$\boldsymbol{y}(t) = \boldsymbol{C}\boldsymbol{x}(t)\,, \tag{3b}$$

where $\boldsymbol{F} \in \mathbb{R}^{8\times8}$, $\boldsymbol{G} \in \mathbb{R}^{8\times3}$, and $\boldsymbol{C} \in \mathbb{R}^{6\times8}$ are the system, input, and output matrices, respectively, see [10].

Finally, as the controller is designed in the discrete-time domain, (3) is discretized with the sampling interval T_s. This yields the discrete-time state-space model of the form [10]

$$\boldsymbol{x}(k+1) = \boldsymbol{A}\boldsymbol{x}(k) + \boldsymbol{B}\boldsymbol{u}_{abc}(k) \tag{4a}$$

$$\boldsymbol{y}(k) = \boldsymbol{C}\boldsymbol{x}(k)\,, \tag{4b}$$

where $k \in \mathbb{N}^+$ denotes the discrete time step.

III. GP^{3}C with Improved Steady-State and Dynamic Behavior

To achieve excellent steady-state and dynamic performance, the GP^{3}C algorithm relies on two key aspects, namely OPPs [8], [9], and gradient-based MPC [15]. In this paper, the GP^{3}C algorithm is revised by further exploiting these two principles. More specifically, optimal output reference trajectories—derived based on the OPP in use—are utilized to ensure the best possible steady-state performance. As for the dynamic performance, a three-phase pulse insertion scheme is introduced which takes advantage of the predictive nature of GP^{3}C, guaranteeing very short transient responses.

A. OPPs for Higher-Order Systems

Conventionally, OPPs are computed by solving an optimization problem such that the TDD of the load current is

minimized. This is done while assuming an inductive load, and by imposing quarter- and half-wave symmetry on the switching signal. The latter implies that only the d switching angles (i.e., switching time instants) occurring within the first quarter of the fundamental period are required to fully describe the OPP. To make OPPs available for the whole operating range and a wide range of switching frequencies, they are computed for the whole range of modulation indices $m \in [0, 4/\pi]$ and different numbers of switching angles. In doing so, several OPPs $\boldsymbol{p}(d, m)$ result.

For higher-order systems, such as the system in Fig. 1, however, the assumption of an inductive load leads to suboptimal pulse patterns, resulting in increased harmonic distortions. To avoid this, the more complex dynamics of the system must be considered in the computation of OPPs. In this paper, this is achieved by considering the transfer function from the switching signal harmonics to the grid current harmonics in the optimization problem [16]. Thereby, optimality—in terms of the grid current TDD—is retained, and harmonic grid codes, such as the IEEE 519 standard [17], are fully respected.

B. Optimal Output Reference Trajectories

OPPs provide the theoretically minimum grid current TDD. Hence, modifying the nominal OPP as little as possible in a closed-loop setting leads to the best possible steady-state performance. This implies that the controller reference trajectory $\boldsymbol{y}_{\text{ref}} = [\boldsymbol{i}_{\text{conv,ref}}^T \ \boldsymbol{i}_{g,\text{ref}}^T \ \boldsymbol{v}_{c,\text{ref}}^T]^T$ should not consider only the fundamental component of the output variables (i.e., to be sinusoidal as in [10]), but it should be computed based on the nominal OPP as this already includes the information about the optimal harmonic content [18].

To compute the optimal reference trajectory for a *single* output $\boldsymbol{\xi}_{\text{ref}}$, with $\boldsymbol{\xi} \in \{\boldsymbol{i}_{\text{conv}}, \boldsymbol{i}_g, \boldsymbol{v}_c\}$, both the fundamental $\boldsymbol{\xi}_{1,\text{ref}}$ and optimal harmonic $\boldsymbol{\xi}_{h,\text{ref}}$ components are required. The former depends on the operating point (i.e., the active P_{ref} and reactive Q_{ref} power requirements). Thus, it can be found by analyzing the steady-state behavior of the system in the rotating (dq) reference plane.

To acquire the latter, harmonic analysis on the OPP $\boldsymbol{u}_{abc}(\theta)$ in use is performed. As a result, the magnitude $\hat{u}_n$ and phase $\hat{\phi}_{u,n}$ of the n^{th} OPP harmonic can be found, where $n = 2\kappa+1$, $\kappa \in \mathbb{N}^+$. Subsequently, the OPP harmonics are mapped into the harmonics of the output $\boldsymbol{\xi}$ with the help of the gain $\hat{g}_{\xi,n}$ and phase shift $\hat{\phi}_{\xi,n}$ of the system resulted from the transfer function $G_\xi(\jmath\omega_g n) = \mathcal{L}\{\boldsymbol{\xi}\}(\jmath\omega_g n)/\mathcal{L}\{\boldsymbol{u}_{abc}\}(\jmath\omega_g n)$. Therefore, with the amplitudes of the output harmonics $\hat{\xi}_n$ and phase shifts $\hat{\phi}_{u,n}$ and $\hat{\phi}_{\xi,n}$, the time-domain optimal harmonic content is derived in an offline procedure according to

$$\xi_{h,\text{ref}}(\theta) = \sum_{n=5,7,\dots,N_{\text{max}}} \hat{\xi}_n \sin(n\theta + \hat{\phi}_{u,n} + \hat{\phi}_{\xi,n}) \,, \quad (5)$$

where $N_{\text{max}} \in \mathbb{N}^+$ is the maximum harmonic order to consider. Note that only the differential-mode harmonics ($n = 5, 7, 11, \dots$) are considered in (5) as the common-mode harmonics do not drive harmonic current.

Finally, the complete optimal reference trajectory $\boldsymbol{\xi}_{\text{ref}}$ is constructed by superimposing the optimal harmonics (5) on the fundamental component, i.e.,

$$\boldsymbol{\xi}_{\text{ref}} = \boldsymbol{\xi}_{1,\text{ref}} + \boldsymbol{\xi}_{h,\text{ref}} \,. \quad (6)$$

It is worth noting that the harmonic analysis is performed offline and the resulting harmonic references are stored in a lookup table (LUT) for all pairs $\{d, m\}$. However, due to the single- and three-phase symmetry properties of the OPP, the harmonic references repeat themselves every $60°$. Hence, it suffices to store the harmonic references for only one sixth of the fundamental period. The complete steady-state reference is then constructed in real time when required by the controller.

C. Control Problem

The control objective of GP^{3}C is to regulate the output $\boldsymbol{y}$ along its *optimal* reference trajectory $\boldsymbol{y}_{\text{ref}}$ (see Section III-B) as fast and as accurately as possible. To this end, the nominal OPP switching time instants that fall within a prediction window $T_p = N_p T_s$ are manipulated in real time, where N_p is the number of prediction horizon time steps. More specifically, given the vector of $z \in \mathbb{N}^+$ nominal OPP switching time instants that fall within the prediction horizon T_p, i.e.,

$$\boldsymbol{t}_{\text{ref}} = \begin{bmatrix} t_{1,\text{ref}} & t_{2,\text{ref}} & \dots & t_{z,\text{ref}} \end{bmatrix}^T \in \mathbb{R}^z \,, \quad (7)$$

GP^{3}C computes the vector of optimally modified switching time instants

$$\boldsymbol{t} = \begin{bmatrix} t_1 & t_2 & \dots & t_z \end{bmatrix}^T \in \mathbb{R}^z \,, \quad (8)$$

such that the desired system behavior is achieved. As shown in [19], the aforementioned control objective is captured in the objective function

$$J = \underbrace{\sum_{i=1}^{z} \|\boldsymbol{y}_{\text{ref}}(t_{i,\text{ref}}) - \boldsymbol{y}(t_i)\|_{\boldsymbol{Q}}^2}_{J_1} + \lambda_t \underbrace{\|\Delta\boldsymbol{t}\|_2^2}_{J_2} \,. \quad (9)$$

The term J_1 in (9) accounts for the (approximate) squared rms output error within the prediction horizon T_p. Additionally, a positive definite weighting matrix $\boldsymbol{Q} = \text{diag}(\boldsymbol{I}_2 q_{\boldsymbol{i}_{\text{conv}}}, \boldsymbol{I}_2 q_{\boldsymbol{i}_g}, \boldsymbol{I}_2 q_{\boldsymbol{v}_c}) \in \mathbb{R}^{6\times 6}$ is used, where $\boldsymbol{I}_2$ is the two-dimensional identity matrix. The diagonal entries of $\boldsymbol{Q}$, where $q_{\boldsymbol{i}_{\text{conv}}}, q_{\boldsymbol{i}_g}, q_{\boldsymbol{v}_c} > 0$, determine the priority among the different tracking terms. As for the term J_2, it models the deviation of the to-be-computed switching time instants from their nominal values, i.e., $\Delta\boldsymbol{t} = \boldsymbol{t}_{\text{ref}} - \boldsymbol{t}$. This term enables the manipulation of the changes in the nominal switching time instants of the (offline-computed) OPP by means of the weighting factor $\lambda_t > 0$.

As can be inferred from (9), the output tracking error is considered only at the nominal OPP switching time instants. Therefore, the system output needs to be predicted at these instants in the horizon. To this aim, the output evolution is computed within the subintervals

$$\Delta t_{\ell,\text{ref}} = t_{\ell+1,\text{ref}} - t_{\ell,\text{ref}} \ll T_1, \ \ell \in \{0, 1, 2, \dots, z-1\} \,, \quad (10)$$

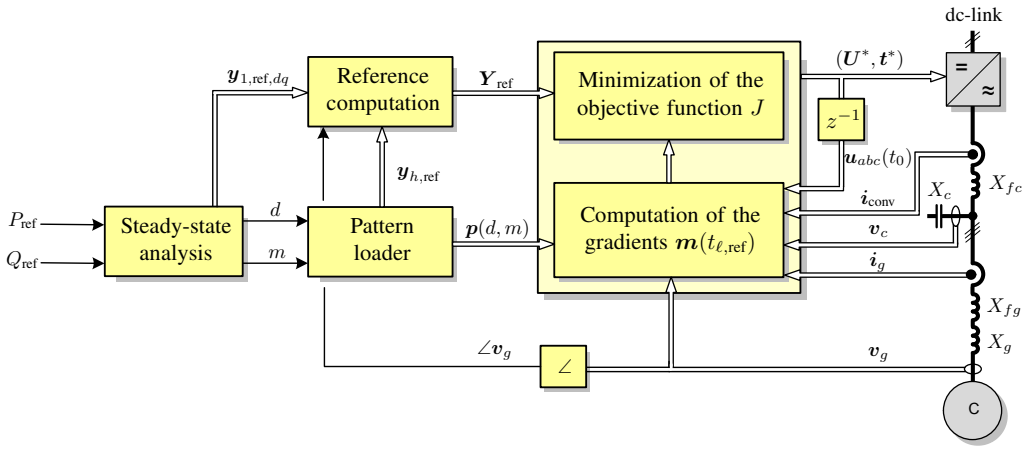

Fig. 3. Block diagram of the proposed control strategy.

where T_1 is the fundamental period, and $t_{0,\text{ref}} \equiv t_0$ is the beginning of the prediction horizon. More specifically, with the knowledge of the current state $\boldsymbol{x}(t_0)$ and the three-phase OPP switch positions, i.e.,

$$\boldsymbol{U} = \begin{bmatrix} \boldsymbol{u}_{abc}^T(t_0) & \boldsymbol{u}_{abc}^T(t_{1,\text{ref}}) & \dots & \boldsymbol{u}_{abc}^T(t_{z,\text{ref}}) \end{bmatrix}^T , \quad (11)$$

the output is predicted at the nominal OPP switching time instants (7). This is done with the discrete-time state-space model (4) in an iterative manner, where the system and input matrices, $\boldsymbol{A}$ and $\boldsymbol{B}$, respectively, are discretized over the subinterval $\Delta t_{\ell,\text{ref}}$.

The knowledge of the output $\boldsymbol{y}(t_{\ell,\text{ref}})$ at the nominal OPP switching time instants facilitates the computation of the output evolution within the subintervals (10) by means of the corresponding gradients $\boldsymbol{m}(t_{\ell,\text{ref}})$. This yields

$$\boldsymbol{m}(t_{\ell,\text{ref}}) = \frac{\mathrm{d}\boldsymbol{y}(t_{\ell,\text{ref}})}{\mathrm{d}t} \approx \frac{\boldsymbol{y}(t_{\ell+1,\text{ref}}) - \boldsymbol{y}(t_{\ell,\text{ref}})}{\Delta t_{\ell,\text{ref}}} . \quad (12)$$

The use of a gradient-based prediction model equips GP^{3}C with high versatility as it enables it to handle non-linear [20] and higher-order [10] systems since the gradients in (12) do not directly depend on the prediction model (4).

Subsequently, with the gradients $\boldsymbol{m}(t_{\ell,\text{ref}})$ (12), the objective function (9) can be written in a vector form

$$J = \|\boldsymbol{r} - \boldsymbol{M}\boldsymbol{t}\|_{\widetilde{\boldsymbol{Q}}}^2 + \lambda_t \|\Delta \boldsymbol{t}\|_2^2 , \quad (13)$$

where vector $\boldsymbol{r} \in \mathbb{R}^{6z}$ depends on the reference and measured values of the output, while the entries of matrix $\boldsymbol{M} \in \mathbb{R}^{6z \times z}$ depend on the aforementioned gradients.[2] It is important to note that the dimensions of vectors $\boldsymbol{r}$, $\boldsymbol{t}$, and matrix $\boldsymbol{M}$ are time-varying as they depend on the number z of switching time instants that fall within the prediction horizon T_p. Finally, the weighting matrix $\widetilde{\boldsymbol{Q}}$ is defined as the block diagonal matrix $\widetilde{\boldsymbol{Q}} = \text{diag}(\boldsymbol{Q}, \boldsymbol{Q}, \dots, \boldsymbol{Q}) \in \mathbb{R}^{6z \times 6z}$.

D. Control Algorithm

In this section, the GP^{3}C algorithm is discussed. The block diagram of the control scheme is shown in Fig. 3, while an algorithmic description is provided in Algorithm 1.

Algorithm 1 GP^{3}C with optimal references

Given $\boldsymbol{x}(t_0)$, $\boldsymbol{y}(t_0)$, $\boldsymbol{u}_{abc}(t_0)$, and $\boldsymbol{p}(m,d)$

0. Extract the three-phase switch positions and corresponding nominal switching time instants that fall within T_p from $\boldsymbol{p}(d,m)$. Construct $\boldsymbol{t}_{\text{ref}}$ and $\boldsymbol{U}$.
1. Retrieve the harmonic references at time instants $\boldsymbol{t}_{\text{ref}}$ from a LUT to generate the output reference trajectory $\boldsymbol{Y}_{\text{ref}}$ within the horizon T_p. Formulate the vector $\boldsymbol{r}$.
2. Predict the system evolution based on (2) and $\boldsymbol{U}$ over the subintervals $\Delta t_{\ell,\text{ref}} = t_{\ell+1,\text{ref}} - t_{\ell,\text{ref}},\ \ell \in \{0,1,2,\dots,z-1\}$
3. Formulate the gradient matrix $\boldsymbol{M}$ based on the gradients $\boldsymbol{m}(t_{\ell,\text{ref}})$.
4. Formulate and solve the QP (15). This yields $\boldsymbol{t}^*$.

Return $\boldsymbol{t}^*(k)$ that fall within T_p and modify the OPP accordingly.

Step 0—*OPP Selection:* In a preprocessing step, the fundamental component of the output reference vector $\boldsymbol{y}_{1,\text{ref},dq}$ is derived while considering the active and reactive power references, P_{ref} and Q_{ref}, respectively, as explained in Section III-B. Subsequently, the resulting fundamental component of the converter voltage $\boldsymbol{v}_{1,\text{conv},dq}$ is used for the computation of the required modulation index m, i.e.,

$$m = \frac{2}{V_{\text{dc}}} \|\boldsymbol{v}_{1,\text{conv},dq}\|_2 . \quad (14)$$

Lastly, the number of switching angles d is chosen. This is done by considering that the switching frequency should be as high as possible—such that the resulting current distortions are kept low—while still remaining below a maximum value $f_{\text{sw,max}}$ and close to the filter resonance frequency f_{res}.[3] The pair $\{d,m\}$ determines the to-be-used OPP $\boldsymbol{p}(d,m)$.

Step 1—*Output Reference Generation:* Following, the desired OPP $\boldsymbol{p}(d,m)$ is retrieved from a LUT, and the switching time instants that fall within the predictions horizon T_p (see (7)) and corresponding three-phase switch positions (see (11)) are extracted. Given $\boldsymbol{t}_{\text{ref}}$, the harmonic reference $\boldsymbol{y}_{h,\text{ref}}$ is retrieved from a LUT while the fundamental component of the reference is acquired by sampling the sinusoidal reference $\boldsymbol{y}_{1,\text{ref}}$. With these, the complete reference is

[2]For a detailed derivation of (13) and the structure of $\boldsymbol{r}$ and $\boldsymbol{M}$ the reader is referred to [10].

[3]The interested readers are referred to [6] for more details.

formed according to (6), providing the output reference vector $\boldsymbol{Y}_{\text{ref}}(k) = [\boldsymbol{y}_{\text{ref}}^T(t_{1,\text{ref}})\ \boldsymbol{y}_{\text{ref}}^T(t_{2,\text{ref}})\ \ldots\ \boldsymbol{y}_{\text{ref}}^T(t_{z,\text{ref}})]^T$.

Step 2—*Optimization Problem:* In a last step, the reference vector $\boldsymbol{r}$ is computed based on $\boldsymbol{Y}_{\text{ref}}$ and the measured state $\boldsymbol{x}(t_0)$. Moreover, with the help of (4), and based on $\boldsymbol{t}_{\text{ref}}$ and $\boldsymbol{U}$, the output gradients $\boldsymbol{m}(t_{\ell,\text{ref}})$ are computed (see (12)) to formulate the gradient matrix $\boldsymbol{M}$.

With the above, the optimization problem

$$\underset{\boldsymbol{t}\in\mathbb{R}^z}{\text{minimize}} \quad \|\boldsymbol{r}-\boldsymbol{M}\boldsymbol{t}\|_{\boldsymbol{Q}}^2 + \lambda_t\|\Delta\boldsymbol{t}\|_2 \tag{15a}$$

$$\text{subject to} \quad kT_s < t_1 < t_2 < \ldots < t_z < kT_s + T_p \tag{15b}$$

is solved, yielding the *optimal* modified switching instants $\boldsymbol{t}^*$. Accordingly, only the modified part of the OPP that falls within the first T_s of T_p is implemented, as per the receding horizon policy [7].

E. Three-Phase Pulse Insertion

The GP^{3}C algorithm can modify only this part of the OPP that falls within the prediction horizon T_p. Therefore, the switch positions that can fully utilize the available voltage margin may not be available to GP^{3}C. This implies that when a change in the demanded power occurs longer settling times, and thus inferior dynamic performance, may result. To address this, and ensure that very fast transient responses can be achieved, the nominal OPP is *locally* overwritten by inserting additional three-phase switch positions that do not (locally) exist in the nominal OPP [11]. As this feature relates to the transient response, it is activated only when the error in the reactive and/or active power exceeds a predetermined limit.

To find the switch position(s) (or, equivalently, voltage vector(s)) that can quickly drive the output to its reference, a simplified system is considered to keep the analysis simple. More specifically, a converter connected to the grid via the reactance $X_{\text{eq}} = X_{fc} + X_{fg} + X_g$ is assumed, while the resistors are considered negligible, see Fig. 4. The dynamics of this system are given by

$$X_{\text{eq}}\frac{\mathrm{d}\boldsymbol{i}_g}{\mathrm{d}t} = \boldsymbol{v}_g - \boldsymbol{v}_{\text{conv}}\,. \tag{16}$$

From (16), it can be deduced that the change in the grid current in one sampling interval T_s is

$$\Delta\boldsymbol{i}_g = \frac{T_s}{X_{\text{eq}}}\left(\boldsymbol{v}_g - \boldsymbol{v}_{\text{conv}}\right). \tag{17}$$

The above implies that the required converter voltage that can quickly reduce the grid current error $\Delta\boldsymbol{i}_g = \boldsymbol{i}_{g,\text{ref}} - \boldsymbol{i}_g$ is

$$\boldsymbol{v}_{\text{conv,ideal}} = \boldsymbol{v}_g - \frac{X_{\text{eq}}}{T_s}\left(\boldsymbol{i}_{g,\text{ref}} - \boldsymbol{i}_g\right). \tag{18}$$

However, as the two-level converter can produce only six discrete active voltage vectors (three-phase switch positions) $\boldsymbol{v}_j$, $j\in\{1,2,\ldots,6\}$, the realizable converter voltage is

$$\boldsymbol{v}_{\text{conv, ins}} = \min\left(\|\boldsymbol{v}_j - \boldsymbol{v}_{\text{conv,ideal}}\|_2\right). \tag{19}$$

However, due to the convoluted system dynamics, and the simplifications during the derivation of (19), the selected

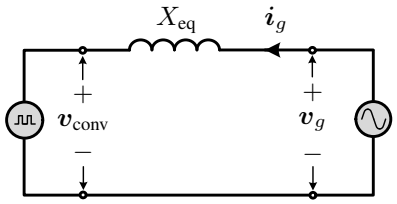

Fig. 4. Equivalent circuit diagram of the simplified system in the stationary orthogonal ($\alpha\beta$) reference frame.

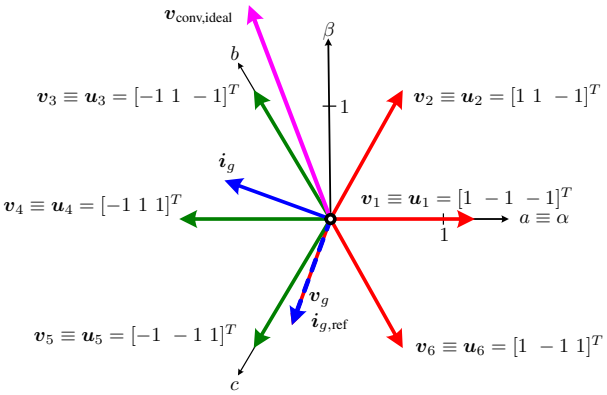

Fig. 5. Example selection of the to-be-inserted three-phase pulses. The grid current vector $\boldsymbol{i}_g$ (blue arrow) is lagging behind its reference $\boldsymbol{i}_{g,\text{ref}}$ (blue dash-dotted arrow) by 90°. The realizable converter voltage vectors $\boldsymbol{v}_j$ and the grid voltage vector $\boldsymbol{v}_g$ are shown as red arrows. The required converter voltage vector $\boldsymbol{v}_{\text{conv,ideal}}$ is shown as a purple arrow. The thee-phase switch positions that will be inserted into the OPP correspond to the converter voltage vectors shown as green arrows.

voltage vector $\boldsymbol{v}_{\text{conv, ins}}$ might not be enough to drive the grid current to its reference. To account for this, and ensure that all the desired three-phase switch positions are available to the controller, the vectors that fall in between $\boldsymbol{v}_{\text{conv, ins}}$ and the grid voltage vector[4] are eventually chosen, see Fig. 4.

In a next step, the selected voltage vector(s) are translated into three-phase switch positions, which are dynamically inserted into the OPP that falls within T_p. This is done in an intuitive manner by exploiting the nature of GP^{3}C. Specifically, the grid current prediction at the previous time step $k-1$ is used to assess if the grid current error convergences monotonically to zero within the prediction horizon. This is done by sampling the magnitude of the predicted grid current error $i_{g,\text{err}} = \|\boldsymbol{i}_{g,\text{ref}} - \boldsymbol{i}_g\|_2$ with the sampling interval $T_c \ll T_s$, and by subsequently observing its evolution at the resulting discrete time steps $p\in\mathbb{N}^+$, i.e.,

$$\boldsymbol{I}_{g,\text{err}} = \begin{bmatrix} i_{g,\text{err}}(p) & i_{g,\text{err}}(p+1) & \ldots & i_{g,\text{err}}(p+m)\end{bmatrix}^T, \tag{20}$$

where $m = (N_p-1)T_s/T_c$. Consequently, since the goal is to have a decreasing grid current error, the difference between every two consecutive current error samples, i.e., entries of $\boldsymbol{I}_{g,\text{err}}$, is required to be negative, implying

$$i_{g,\text{err}}(p+\ell) - i_{g,\text{err}}(p+\ell-1) < 0,\ \ell\in\{1,2,\ldots,m\}. \tag{21}$$

Hence, the chosen three-phase pulses are added to the OPP at the time instant $t_{\text{ins}} = kT_s + \ell T_c$ of the prediction horizon

[4]Note that, as per (18), $\boldsymbol{v}_{\text{conv, ins}} = \boldsymbol{v}_g$ implies a zero grid current error.

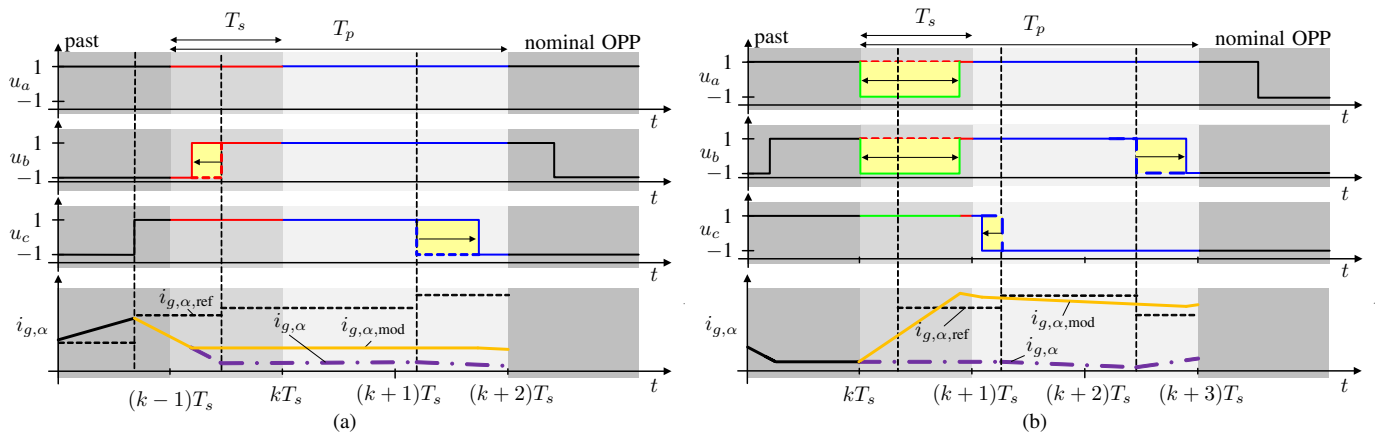

Fig. 6. Example of three-phase pulse insertion. Gradient-based evolution of the α-component of the grid current $i_{g,\alpha}$ at time step (a) $k-1$, and (b) k. The optimal modifications to the nominal OPP (dash-dotted line) are shown with arrows and the added/removed volt-seconds are highlighted. The to-be-implemented pulse pattern is shown in red while the remaining part of the OPP that falls into the prediction horizon is shown in blue. The modifications resulting from the three-phase pulse insertion are shown in green.

where condition (21) is violated for the first time. These three-phase switch positions are inserted into the OPP as pulses of infinitesimal width. Following, GP^{3}C manipulates them such that the output tracking error is eliminated. It is worth mentioning, however, that the inserted three-phase pulses that are ineffective in one controller iteration, i.e., they are not used by GP^{3}C, they are removed in the subsequent iteration. This is done to avoid an excessive number of additional pulses that would significantly increase the size of the optimization problem and could potentially lead to chattering.

To better understand the concept of the three-phase pulse insertion, the following example is provided.

Example 1: *Consider the system in Fig. 1 controlled by GP^{3}C with a three-step horizon ($N_p = 3$). Fig. 6(a) depicts the nominal OPP, the optimal modifications, and the evolution of the α-component of the grid current $i_{g,\alpha}$ at time step $k-1$. As can be seen, the existing OPP switch positions do not facilitate the elimination of the grid current error, despite the control actions of GP^{3}C. Therefore, condition* (21) *is violated at time step k, meaning that three-phase pulses of infinitesimal width are inserted into the nominal OPP. Subsequently, the GP^{3}C optimization problem* (15) *is solved, and the (nominal OPP and inserted) switching time instants are modified in an optimal manner. As can be seen from Fig. 6(b), pulse $[-1 \;\; -1 \;\; 1]^T$ is preferred out of all the inserted three-phase pulses, i.e., it is widened to eliminate the grid current reference tracking error. On the other hand, the unused inserted pulses are removed. As a result of the insertion, the controller can quickly drive $i_{g,\alpha}$ towards its reference.*

IV. Performance Evaluation

This section assesses the performance of GP^{3}C with the system shown in Fig. 1. The rated values and parameters of the system are provided in Tables I and II, respectively. The filter parameters result in a resonance frequency of $f_{\text{res}} = 892\,\text{Hz}$. As for the controller parameters, the sampling interval is $T_s = 50\,\mu\text{s}$ and $N_p = 10$. The weighting matrix $\boldsymbol{Q}$ is chosen as the identity matrix, while $\lambda_t = 1 \cdot 10^6$. A two-level OPP with a number of switching angles $d = 15$ is used such that the device switching frequency is $f_{\text{sw}} = 1550\,\text{Hz}$, and the modulation index is $m = 1.042$ at nominal operating conditions. Finally, all results are shown in the per unit (p.u.) system.

TABLE I
RATED VALUES OF THE SYSTEM

Parameter	Symbol	SI value
Voltage	V_R	400 V
Current	I_R	18 A
Power	P_R	12.5 kVA
Grid frequency	f_R	50 Hz

TABLE II
SYSTEM PARAMETERS

Subject	Parameter	Symbol	p.u. value
LCL filter	Converter-side resistance	R_{fc}	$7.7942 \cdot 10^{-3}$
	Grid-side resistance	R_{fg}	$5.4559 \cdot 10^{-3}$
	Capacitor resistance	R_c	$0.0624 \cdot 10^{-3}$
	Converter-side reactance	X_{fc}	0.1616
	Grid-side reactance	X_{fg}	0.1469
	Capacitor reactance	X_c	28.1930
Grid	Grid resistance	R_g	0.0071
	Grid reactance	X_g	0.0490
Converter	Dc-link voltage	V_{dc}	1.9902

The steady-state performance of the proposed GP^{3}C scheme is shown in Fig. 7 for operation at nominal conditions ($P_{\text{ref}} = 1\,\text{p.u.}$ and $Q_{\text{ref}} = 0\,\text{p.u.}$). As can be seen, the active and reactive power references are successfully tracked. Moreover, thanks to the optimal reference trajectories, the controller does not take unnecessary actions at steady-state operation, meaning that the applied switching pattern deviates from the nominal OPP as little as possible. As a result, the grid current TDD is only 0.33%, i.e., very close to that produced by the nominal OPP. Moreover, the current harmonics are located at odd, non-triplen integer multiples of the fundamental frequency, see Fig. 7(e), thus supporting adherence to harmonic grid standards, such as the IEEE 519 standard.

To better elucidate the superior steady-state performance of the proposed controller, Fig. 8 compares the grid current TDD that results from conventional linear control with SVM,

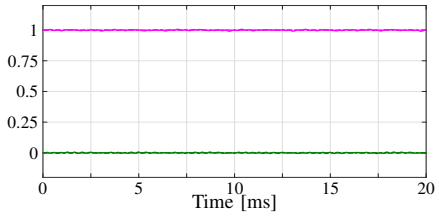

(a) Active P (magenta) and reactive power Q (green) and their references (dash-dotted line).

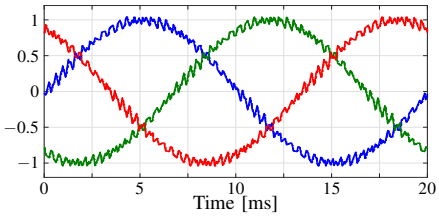

(b) Three-phase converter currents $\boldsymbol{i}_{\text{conv},abc}$ (solid lines) and their references (dash-dotted lines).

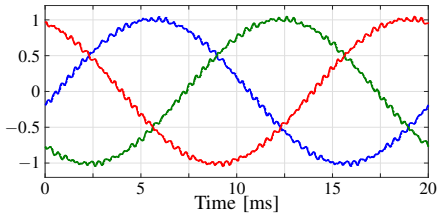

(c) Three-phase capacitor voltages $\boldsymbol{v}_{c,abc}$ (solid lines) and their references (dash-dotted lines).

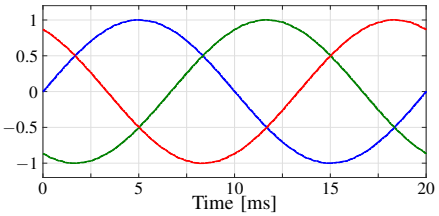

(d) Three-phase grid currents $\boldsymbol{i}_{g,abc}$ (solid lines) and their references (dash-dotted lines).

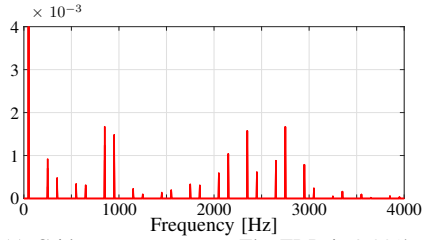

(e) Grid current spectrum. The TDD is 0.33%.

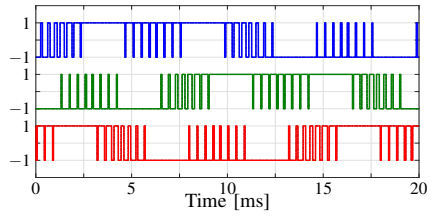

(f) Three-phase (modified) switching pattern $\boldsymbol{u}_{abc}$ (solid lines) and nominal OPP (dash-dotted lines).

Fig. 7. Simulation results of GP^{3}C with optimal output reference trajectories during steady-state operation and unity power factor ($f_{\text{sw}} = 1550\,\text{Hz}$).

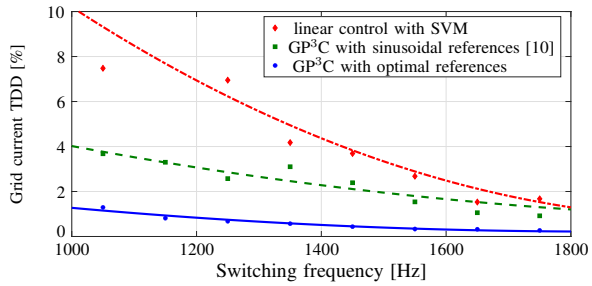

Fig. 8. Grid current TDD for GP^{3}C with optimal and sinusoidal reference trajectories, and linear control with SVM.

GP^{3}C with sinusoidal references [10], and the improved GP^{3}C scheme proposed in this work over a range of switching frequencies. As can be seen, the proposed controller not only produces the lowest grid current TDD over the whole range of examined switching frequencies, but it is also at least three and five times, respectively, lower than that of GP^{3}C from [10] and linear control with SVM.

Finally, the transient performance of the system is shown in Fig. 9, where P_{ref} is stepped up from 0 to 1 p.u. and Q_{ref} is stepped down from 1 to 0 p.u. at $t = 2\,\text{ms}$. Therein, the dynamic behavior of the proposed controller is compared with that of GP^{3}C without three-phase pulse insertion and FCS-MPC [13]. As can be seen in Figs. 9(a) and 9(b), the three-phase pulse insertion can drastically speed up the response time of GP^{3}C and reduce the oscillations. Inserted pulses can be identified, e.g., in phase a around $t = 4\,\text{ms}$, where the switch position $u_a = 1$ is inserted. It is worth mentioning that the additional pulses only marginally increase the switching frequency, while chattering is avoided altogether. More interestingly, thanks to the pulse insertion, GP^{3}C can achieve settling times on par with FCS-MPC, see Fig. 9(c). The latter being a direct—and thus very aggressive—control method, can achieve the fastest possible transient responses. Thus, the presented results clearly demonstrate the excellent dynamic performance of the proposed GP^{3}C scheme.

V. Conclusions

This work improved the steady-state and dynamic behavior of the GP^{3}C algorithm presented in [10]. To achieve the former, optimal reference trajectories are derived for the controlled variables by performing harmonic analysis on the OPP in use. By using these trajectories in the GP^{3}C setting, unnecessary control actions are avoided since the optimal output ripple is already accounted for. Thereby, excellent steady-state performance is achieved, resulting in a grid current TDD very close to its theoretically minimum value. As for the latter, a three-phase pulse insertion strategy is employed to locally overwrite the OPP during transients by strategically adding pulses to the OPP. In doing do, the available voltage margin is fully utilized, while chattering is avoided. Consequently, this mechanism enables GP^{3}C to achieve very fast transient responses, comparable to those of FCS-MPC, as shown with the presented results.

Acknowledgment

This work was supported by the Research Council of Finland.

References

[1] M. Liserre, F. Blaabjerg, and S. Hansen, "Design and control of an LCL-filter-based three-phase active rectifier," *IEEE Trans. Ind. Appl.*, vol. 41, no. 5, pp. 1281–1291, Sep./Oct. 2005.

[2] P. C. Loh and D. G. Holmes, "Analysis of multiloop control strategies for $LC/CL/LCL$-filtered voltage-source and current-source inverters," *IEEE Trans. Ind. Appl.*, vol. 41, no. 2, pp. 644–654, Mar./Apr. 2005.

[3] D. G. Holmes and T. A. Lipo, *Pulse width modulation for power converters: Principles and practice*. Piscataway, NJ, USA: IEEE Press, 2003.

[4] J. Dannehl, F. W. Fuchs, S. Hansen, and P. B. Thøgersen, "Investigation of active damping approaches for PI-based current control of grid-connected pulse width modulation converters with LCL filters," *IEEE Trans. Ind. Appl.*, vol. 46, no. 4, pp. 1509–1517, Jul./Aug. 2010.

[5] S. G. Parker, B. P. McGrath, and D. G. Holmes, "Regions of active damping control for LCL filters," *IEEE Trans. Ind. Appl.*, vol. 50, no. 1, pp. 424–432, Jan./Feb. 2014.

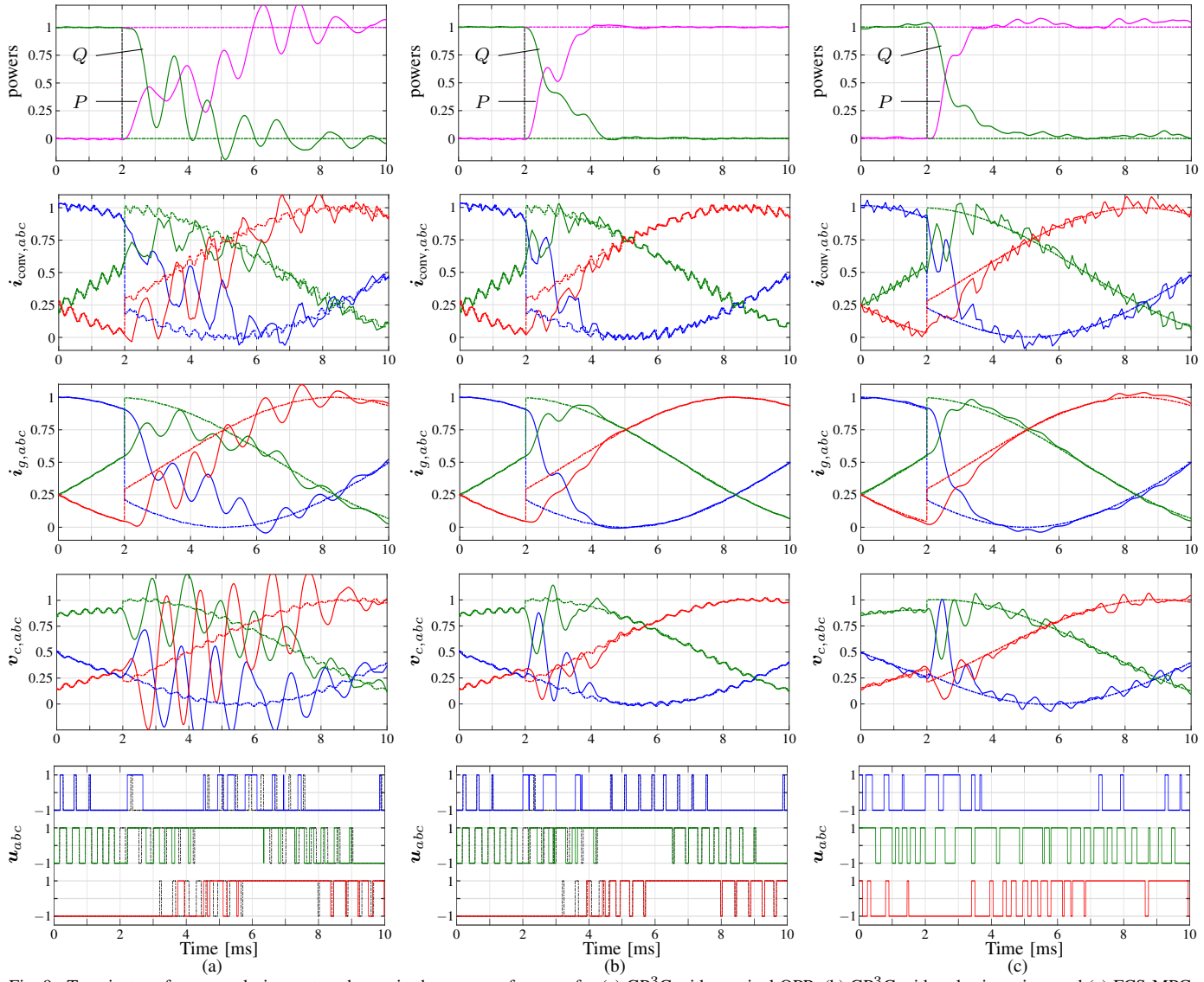

Fig. 9. Transient performance during a step change in the power references for (a) GP^{3}C with nominal OPP; (b) GP^{3}C with pulse insertion; and (c) FCS-MPC.

[6] T. Geyer, N. Oikonomou, G. Papafotiou, and F. D. Kieferndorf, "Model predictive pulse pattern control," *IEEE Trans. Ind. Appl.*, vol. 48, no. 2, pp. 663–676, Mar./Apr. 2012.

[7] J. B. Rawlings and D. Q. Mayne, *Model Predictive Control: Theory and Design*. Madison, WI: Nob Hill, 2009.

[8] G. S. Buja and G. B. Indri, "Optimal pulsewidth modulation for feeding ac motors," *IEEE Trans. Ind. Appl.*, vol. IA-13, no. 1, pp. 38–44, Jan./Feb. 1977.

[9] G. S. Buja, "Optimum output waveforms in PWM inverters," *IEEE Trans. Ind. Appl.*, vol. IA-16, no. 6, pp. 830–836, Nov./Dec. 1980.

[10] P. Karamanakos, M. A. W. Begh, S. Rahmanpour, and T. Geyer, "Gradient-based predictive pulse pattern control for grid-connected converters with LCL filters," in *Proc. IEEE Energy Convers. Congr. Expo.*, Nashville, TN, USA, Oct. 2023, pp. 2645–2652.

[11] T. Geyer and N. Oikonomou, "Model predictive pulse pattern control with very fast transient responses," in *Proc. IEEE Energy Convers. Congr. Expo.*, Pittsburgh, PA, USA, Sep. 2014, pp. 5518–5524.

[12] J. Dannehl, C. Wessels, and F. W. Fuchs, "Limitations of voltage-oriented PI current control of grid-connected PWM rectifiers with LCL filters," *IEEE Trans. Ind. Electron.*, vol. 56, no. 2, pp. 380–388, Feb. 2010.

[13] J. Rodríguez and P. Cortés, *Predictive control of power converters and electrical drives*. Chichester, UK: Wiley, 2012.

[14] S. Kouro, M. A. Perez, J. Rodríguez, A. M. Llor, and H. A. Young, "Model predictive control: MPC's role in the evolution of power electronics," *IEEE Ind. Electron. Mag.*, vol. 9, no. 4, pp. 8–21, Dec. 2015.

[15] P. Karamanakos, M. Nahalparvari, and T. Geyer, "Fixed switching frequency direct model predictive control with continuous and discontinuous modulation for grid-connected converters with LCL filters," *IEEE Trans. Control Syst. Technol.*, vol. 29, no. 4, pp. 1503–1518, Jul. 2021.

[16] L. G. Franquelo, J. Nápoles, R. C. P. Guisado, J. I. León, and M. A. Aguirre, "A flexible selective harmonic mitigation technique to meet grid codes in three-level PWM converters," *IEEE Trans. Ind. Electron.*, vol. 54, no. 6, pp. 3022–3029, Dec. 2007.

[17] IEEE Std 519-2014 (Revision of IEEE Std 519-1992), "IEEE recommended practices and requirements for harmonic control in electrical power systems," pp. 1–29, Jun. 2014.

[18] J. Holtz and B. Beyer, "Fast current trajectory tracking control based on synchronous optimal pulsewidth modulation," *IEEE Trans. Ind. Appl.*, vol. 31, no. 5, pp. 1110–1120, Sep./Oct. 1995.

[19] M. A. W. Begh, P. Karamanakos, and T. Geyer, "Gradient-based predictive pulse pattern control of medium-voltage drives—Part I: Control, concept, and analysis," *IEEE Trans. Power Electron.*, vol. 37, no. 12, pp. 14 222–14 236, Dec. 2022.

[20] ——, "Gradient-based predictive pulse pattern control with active neutral point potential balancing for medium-voltage induction motor drives," *IEEE Trans. Ind. Appl.*, vol. 60, no. 4, pp. 6326–6338, Jul./Aug. 2024.